

## NOTE TO USERS

PREVIEW

This reproduction is the best copy available.

**UMI**<sup>®</sup>

PREVIEW

CRYSTAL STRUCTURE, MICROSTRUCTURE AND  
MAGNETIC PROPERTIES OF RAPIDLY SOLIDIFIED  
SAMARIUM-COBALT BASED ALLOYS

By

Shampa Aich

A DISSERTATION

Presentated to the Faculty of

The Graduate College at the University of Nebraska

In Partial Fulfilment of Requirements

For the degree of Doctor of Philosophy

Major: Engineering (Chemical and Materials Engineering)

Under the Supervision of Professor Jeffrey E. Shield

Lincoln, Nebraska

August, 2005

UMI Number: 3186845

### INFORMATION TO USERS

The quality of this reproduction is dependent upon the quality of the copy submitted. Broken or indistinct print, colored or poor quality illustrations and photographs, print bleed-through, substandard margins, and improper alignment can adversely affect reproduction.

In the unlikely event that the author did not send a complete manuscript and there are missing pages, these will be noted. Also, if unauthorized copyright material had to be removed, a note will indicate the deletion.

**UMI<sup>®</sup>**

---

UMI Microform 3186845

Copyright 2005 by ProQuest Information and Learning Company.

All rights reserved. This microform edition is protected against unauthorized copying under Title 17, United States Code.

ProQuest Information and Learning Company  
300 North Zeeb Road  
P.O. Box 1346  
Ann Arbor, MI 48106-1346

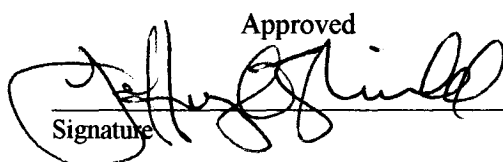
DISSERTATION TITLE

Crystal Structure, Microstructure And Magnetic Properties Of Rapidly Solidified Samarium-  
Cobalt-Based Alloys

BY

Shampa Aich

SUPERVISORY COMMITTEE:

Approved  
  
Signature

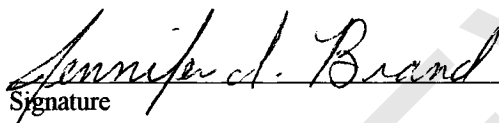
Jeffrey E. Shield  
Typed Name

Date  
5/20/05

  
Signature


Brian W. Robertson  
Typed Name

5/20/05

  
Signature

Jennifer I. Brand  
Typed Name

05/20/05

  
Signature

Diandra Leslie-Pelecky  
Typed Name

5/20/05

Signature

Typed Name

Signature

Typed Name

UNIVERSITY OF  
**Nebraska**  
Lincoln

# CRYSTAL STRUCTURE, MICROSTRUCTURE AND MAGNETIC PROPERTIES OF RAPIDLY SOLIDIFIED SAMARIUM-COBALT BASED ALLOYS

Shampa Aich, Ph.D

University Of Nebraska – Lincoln, 2005

Advisor: Dr. Jeffrey E. Shield

The SmCo-based permanent magnets are drawing much more attention since the early 1970's for their highly attractive features such as, high energy product (15 MGOe–30 MGOe), reliable coercive force, best temperature characteristics and excellent corrosion and oxidation resistance. These interesting and highly demanding features have made Sm-Co the ideal material in dynamic applications such as generators and motors. The melt-spun ribbons of Sm-Co-based magnetic materials produced by rapid solidification exhibited higher anisotropy, improved microstructures and better magnetic properties ( $M_r \sim 8.5$  kG,  $H_c \sim 4.1$  kOe and  $(BH)_{\max} \sim 18.2$  MGOe and a high remanence ratio of 0.9).

This research reports the structure and magnetic properties of rapidly solidified Sm-Co permanent magnets of simple binary alloy systems modified with Nb and C additions. Melt spinning at 40 m/s resulted in the formation of the metastable TbCu<sub>7</sub>-type structure in all instances regardless of alloying additions. While the unalloyed Sm<sub>12</sub>Co<sub>88</sub> alloy displayed a coercivity of 0.5 kOe, alloying additions resulted in a systematic and profound increase in coercivity, with maximum values exceeding 37 kOe. TEM revealed the presence of fcc Co, formed as a result of the non-equilibrium processing. The

alloying additions had a profound influence on the scale of the microstructure, reducing the  $\text{SmCo}_7$  grains from the micron-scale to the 100 nm range and the scale of the Co from 80 nm to 10 nm. The nanoscale Co soft magnetic phase enables exchange coupling to the hard magnetic phase, resulting in high remanence ratios ( $\sim 0.7$ ).

For a range of compositions, from  $\text{SmCo}_{5.67}$  to  $\text{SmCo}_8$ , the coercivity was highest in Sm-rich compositions (17.5 kOe) and decreased to  $\sim 3$  kOe as Sm content decreased.

At higher wheel speed during melt-spinning, the higher chances of formation of Co precipitate and the reduced size of Co precipitates helped to improve the remanence. At higher wheel speed and at higher concentration of alloying additions the magnetization process was dominated by pinning mechanism.

During the order-disorder phase transformations, the as-solidified alloys in the  $\text{TbCu}_7$ -type structure exhibited coercivity as high as 7.85 kOe, which increased to greater than 9 kOe by heat-treatment. The magnetization processes were also strongly influenced by the structural state during order-disorder phase transformations, initially it was totally controlled by nucleation followed by the domain wall pinning.

## TABLE OF CONTENTS

<b>ABSTRACT .....</b>	<b>i</b>
<b>TABLE OF CONTENTS .....</b>	<b>iii</b>
<b>LIST OF FIGURES .....</b>	<b>vi</b>
<b>LIST OF TABLES .....</b>	<b>xiv</b>
<b>ACKNOWLEDGMENTS .....</b>	<b>xv</b>
<b>Chapter</b>	
<b>1. INTRODUCTION.....</b>	<b>1</b>
1.1 Significance of the Study .....	1
1.2 Objectives ... ..	6
1.3 References .....	8
<b>2. THEORETICAL ASPECTS.....</b>	<b>9</b>
2.1 Fundamentals of Magnetism in Materials.....	9
2.2 Different Types of Magnetic Materials.....	10
2.2.1 Diamagnetic Materials .....	10
2.2.2 Paramagnetic Materials.....	11
2.2.3 Ferromagnetic Materials .....	12
2.2.4 Antiferromagnetic Materials.....	12
2.2.5 Ferrimagnetic Materials .....	13
2.3 Magnetization Curves and Hysteresis Loops.....	14
2.4 Classification Of Hard and Soft Magnetic Materials.....	17
2.5 Magnetic Anisotropy .....	19
2.5.1 Magnetocrystalline Anisotropy.....	21
2.5.1.1 Cubic Anisotropy .....	21
2.5.1.2 Uniaxial Anisotropy.....	23
2.5.2 Shape Anisotropy.....	26
2.5.3 Stress Anisotropy .....	29
2.5.4 Exchange Anisotropy .....	31
2.6 Magnetic Domains and Domain Walls .....	32
2.7 Single Domain Particles / Multi Domain Particles .....	35
2.8 Magnetization Process :: Nucleation/Pinning.....	37
2.9 Magnetization Reversal .....	41
2.9.1 Magnetization Reversal By Coherent Rotation .....	41
2.9.2 Magnetization Reversal By Incoherent Rotation.....	43



2.9.2.1	Fanning .....	44
2.9.2.2	Curling and Buckling.....	45
2.9.3	Magnetization Reversal By Domain Wall Nucleation.....	47
2.9.4	Magnetization Reversal By Domain Wall Pinning.....	50
2.10	References.....	54
<b>3.</b>	<b>RARE-EARTH PERMANENT MAGNETS.....</b>	<b>58</b>
3.1	Permanent Magnets.....	58
3.1.1	Historical Review.....	58
3.1.2	Applications .....	64
3.2	Rare-Earth – Coupled With A Non-magnetic Partner .....	65
3.3	Rare-Earth – Transition Metal Systems.....	67
3.2	Rare-Earth – Cobalt Systems.....	65
3.2.1	RCo <sub>5</sub> Systems.....	68
3.2.1.1	Crystal Structures.....	70
3.2.1.2	Magnetic Properties .....	70
3.2.2	R <sub>2</sub> Co <sub>17</sub> Systems.....	71
3.2.2.1	Crystal Structures.....	71
3.2.2.2	Magnetic Properties .....	74
3.4	Sm-Co Based Permanent Magnets (Sintered / Bonded).....	75
3.4.1	Phase Stability in Sm-Co Systems.....	78
3.4.2	Crystal Structures of Sm-Co Systems.....	79
3.4.2.1	SmCo <sub>5</sub> Structure.....	80
3.4.2.2	Sm <sub>2</sub> Co <sub>17</sub> Structure.....	80
3.4.2.3	SmCo <sub>7</sub> Structure.....	80
3.4.3	Magnetic Properties of Sm-Co Alloys.....	81
3.4.3.1	The Intermetallic Compound SmCo <sub>5</sub> .....	82
3.4.3.2	Sm <sub>2</sub> Co <sub>17</sub> -based Permanent Magnets .....	85
3.4.4	Sm-Co Alloys Produced by Rapid Solidifications.....	88
3.5	References.....	96
<b>4.</b>	<b>EXPERIMENTAL PROCEDURE .....</b>	<b>100</b>
4.1	Materials Selection.....	100
4.2	Compositions Studied .....	101
4.3	Sample Preparation Techniques.....	101
4.3.1	Arc-Melting.....	101
4.3.2	Melt-Spinning .....	103
4.3.3	Annealing.....	109
4.4	Sample Characterization Methods .....	109
4.4.1	X-Ray Diffraction .....	109
4.4.2	Transmission Electron Microscopy .....	114
4.4.3	Grain Size Measurement.....	121
4.4.4	Vibrating Sample Magnetometer.....	122
4.4.5	SQUID Magnetometer .....	124

4.4.6 Recoil Measurements.....	129
4.5 References.....	132
<b>5. RESULTS &amp; DISCUSSIONS .....</b>	<b>134</b>
5.1 Effect of Additives.....	134
5.1.1 Effect of Nb Substitution on $\text{Sm}_{12}\text{Co}_{88}$ Alloys .....	134
5.1.1.1 Phase Formations.....	135
5.1.1.2 Microstructures .....	135
5.1.1.3 Magnetic Properties .....	137
5.1.2 Effect of C Substitution on $\text{Sm}_{12}\text{Co}_{88}$ Alloys.....	143
5.1.2.1 Phase Formations.....	143
5.1.2.2 Microstructures .....	145
5.1.2.3 Magnetic Properties .....	150
5.1.3 Effect of Nb and C Substitution on $\text{Sm}_{12}\text{Co}_{88}$ Alloys.....	154
5.1.3.1 Phase Formations.....	154
5.1.3.2 Microstructures .....	157
5.1.3.3 Magnetic Properties .....	160
5.1.4 Summary.....	169
5.2 Effect of Wheel Speed .....	170
5.2.1 Phase Formations.....	170
5.2.2 Microstructures .....	170
5.2.3 Magnetic Properties .....	173
5.2.4 Summary.....	178
5.3 Effect of Compositions .....	178
5.3.1 Phase Formations.....	179
5.3.2 Microstructures .....	183
5.3.3 Magnetic Properties .....	185
5.3.4 Summary.....	190
5.4 Heat-treatment of Rapidly Solidified Sm-Co Alloys.....	191
5.4.1 Phase Formation.....	191
5.4.2 Microstructures .....	196
5.4.3 Magnetic Properties .....	198
5.4.4 Summary.....	211
5.5 References.....	213
<b>6. CONCLUSIONS .....</b>	<b>214</b>
6.1 Effect of Additives.....	214
6.2 Effect of Composition.....	214
6.3 Heat-treatment of Rapidly Solidified Sm-Co Alloys.....	215

## LIST OF FIGURES

2.1	Different kinds of magnetic behaviour observed in a material: (a) paramagnetic, (b) ferromagnetic, (c) antiferromagnetic and (d) ferrimagnetic .....	14
2.2	Hysteresis loop of a magnetic material (adapted from [13]). .....	16
2.3	Typical magnetization curves for (a) diamagnetic and (b) paramagnetic material and © vacuum (adapted from [14]).....	17
2.4	Schematic magnetization curves for (a) soft and (b) hard magnetic materials (adapted from [15]). .....	18
2.5	Effect of internal stress/strain in a magnetic material (adapted from [16]) .....	19
2.6	Hard and easy directions for magnetization for (a) bcc Fe and (b) fcc Ni with their corresponding magnetization curves (adapted from [19]). .....	22
2.7	Polar coordinates considering a uniaxial system (adapted from [20]).....	23
2.8	Hard and easy directions for magnetization for hcp Co with their corresponding magnetization curves (adapted from [19]). .....	25
2.9	Shape anisotropy in polar coordinates (a) prolate spheroid and (b) oblate spheroid (adapted from [24,25]).....	28
2.10	The shape anisotropy in a prolate ellipsoid of revolution showing the dependence of the difference between the two principal demagnetization factor on the axial ratio $a/b$ (adapted from [27]).....	29
2.11	Reduction of the magnetostatic energy associated with the leakage of the magnetic flux due to formation of domain structure by dividing the domains (adapted from [31]). .....	32
2.12	Magnetic domain structures (a) MFM image of heat-treated carbon steel, (b) 'Fir-tree' domains on a (100) surface of a 3.2% Si-Fe crystal and (c) Basal plane domains of a hexagonal $\text{SmCo}_5$ crystal (adapted from [33, 34]).....	33
2.13	Structure of a $180^\circ$ magnetic domain wall (adapted from [31]). .....	34

2.14	Relation between the energy $E$ of a crystal and its thickness $L$ for two kinds of magnetic state (adapted from [38]).....	37
2.15	The domain wall energy ( $\gamma$ ) as a function of the position ( $x$ ) in a magnetic material showing the pinning sites and the barriers for the domain wall (adapted from [40]).....	39
2.16	Initial magnetization curves for different materials (adapted from [43]).....	40
2.17	Magnetization reversal in a single-domain particle by coherent rotation mechanism.....	42
2.18	Magnetization reversal by fanning.....	44
2.19	Magnetization reversal by curling (adapted from [53, 54]).....	45
3.1	Typical demagnetization curves for the most important permanent magnets [1].....	59
3.2	Equal energy output for materials having different volume.....	60
3.3	The demagnetization quadrant of a typical permanent magnet material and the variation of $(BH)$ product with the demagnetizing field [2].....	60
3.4	Improvements in $(BH)_{\max}$ for permanent magnets since 1900 [3].....	61
3.5	(a) Permanent magnets applications, according to sales statistics, (b) Sales distribution of permanent magnets and (c) Applications of Sm-Co magnets [12].....	66
3.6	The $\text{CaCu}_5$ -type $\text{RCo}_5$ hexagonal crystal structure [10].....	70
3.7	Polymorphic forms of $\text{R}_2\text{Co}_{17}$ compounds at different temperatures [24].....	74
3.8	Sm-Co-based Magnets [36].....	77
3.9	Equilibrium Phase Diagram of Sm-Co System [37].....	79
3.10	The crystal structures of Sm-Co phases (a) $\text{Sm}_2\text{Co}_{17}$ and (b) $\text{SmCo}_7$ [40].....	81
3.11	The magnetization curves for single crystal $\text{SmCo}_5$ parallel and perpendicular to the easy axis of magnetization [42].....	82
3.12	Domain walls pinned by an $\text{Sm}(\text{Co}, \text{Cu})_5$ , (1:5) phase: (a) in a plane	

	perpendicular to the easy hexagonal [0001] axis and (b) in a plane parallel to the easy hexagonal [0001] axis [65].....	86
3.13	Detailed microstructure of the rhombic cells. AB represents a domain wall pinned or blocked by the $\text{Sm}(\text{Co}, \text{Cu})_5$ boundary phase [66].....	87
3.14	The dependence of the coercivity of $\text{Sm}(\text{Co}_{0.74}\text{Fe}_{0.1}\text{Zr}_{0.04}\text{Cu}_{0.12})_8$ as-spun samples on the wheel velocity [81].....	91
3.15	TEM micrographs of $\text{Sm}(\text{Co}_{0.74}\text{Fe}_{0.1}\text{Zr}_{0.04}\text{Cu}_{0.12})_8$ ribbons melt-spun at 53 m/s: (a) as-spun and (b) annealed at 750°C for 40 minutes and melt-spun at 26 m/s: (c) as-spun and (d) annealed at 750°C for 60 minutes [81].....	92
3.16	Bright field image of (a) $\text{Sm}(\text{CoFeCuZr})_{7.7}\text{B}_{1.0}$ annealed at 700°C consisting of a mixture of 2:17 and $\alpha$ -Fe with a grain size of 30-50 nm and (b) $\text{Sm}(\text{CoFeCuZrC}_{0.1})_{8.5}$ with an average grain size of 100 nm [83].....	95
4.1	Arc melting furnace (adapted from [1]).....	103
4.2	Cooling and Solidification of a sphere or a cylinder or a slab. The arrows are indicating the direction of heat extraction [adapted from 5].....	105
4.3	Melt-spinner furnace.....	107
4.4	Melt-spun ribbons.....	108
4.5	Electronic transitions in an atom indicating the emission processes by arrows (adapted from [7]).....	111
4.6	The fine structure of the L state (adapted from [8]).....	112
4.7	Diffraction of x-rays by a crystal (adapted from [9]).....	112
4.8	Schematic representation of X-ray Diffractometer (adapted from [12]).....	114
4.9	Schematic representation of a Transmission Electron Microscope (adapted from [13]).....	117
4.10	Ray diagrams for the two basic imaging modes of the TEM : (a) Bright Field and (b) Dark Field (adapted from [15]).....	119
4.11	Ray diagrams for the two basic operation modes of the TEM : Projection of (a) the diffraction pattern and (b) the image on the viewing screen (adapted from [16]).....	121

4.12	Schematic of the Vibrating Sample Magnetometer (adpted from [17, 18]).....	123
4.13	Schematic of the Vibrating Sample Magnetometer (adpted from [17, 18]).....	125
4.14	Schematic of the Vibrating Sample Magnetometer (adpted from [17, 18]).....	127
4.15	Illustration of an RSO measurement : (a) an ideal SQUID response, (b) the movement of the sample inside a SQUID pick-up coil (adapted from [22]).....	128
4.16	Definition of $M_{irr}$ and $M_{rev}$ and the procedure adapted to analyze the recoil data (adapted from [25]).....	130
5.1	X-ray diffraction scans of $(Sm_{12}Co_{88})_{100-x}Nb_x$ alloy melt spun at 40 m/s for $x = 0, 1, 2, 3$ and $5$ (from (a) to (e)). Peaks were indexed to the $SmCo_7$ structure.....	136
5.2	Transmission electron micrographs revealing the microstructure of the $(Sm_{12}Co_{88})_{100-x}Nb_x$ alloy melt-spun at 40 m/s (a) $x=0$ showing micron size grain, (b) for $x=1$ showing equiaxed smaller 1:7 grains and (c) for $x=3$ showing similar kind of grain structure and grain size like $x=1$ and (d) for $x=5$ showing equiaxed 1:7 grains relatively smaller in size with a few scatterd black spots.....	138
5.3	Transmission electron micrographs revealing the microstructure of the $(Sm_{12}Co_{88})_{100-x}Nb_x$ alloy melt-spun at 40 m/s (a) for $x=1$ showing columnar 1:7 grains and (b) for $x=5$ showing polygonal grains.....	139
5.4	Hysteresis loops of $(Sm_{12}Co_{88})_{100-x}Nb_x$ alloy melt spun at 40 m/s for $x = 0, 1, 2, 3$ and $5$ .....	140
5.5	Relationship between %additives ( $x$ ,) and intrinsic coercivity for the $Sm_{12}Co_{88}$ alloys – 40 m/s modified with Nb ( $\blacktriangle$ ).....	141
5.6	The normalised curves showing initial magnetization processes for the $(Sm_{12}Co_{88})_{100-x}Nb_x$ -40m/s alloys at different $x$ values, $x=1$ ( $\blacklozenge$ ), $x=2$ ( $\blacktriangle$ ), $x=3$ ( $\blacksquare$ ) and $x=5$ ( $\times$ ). The curve (+) is indicating the sample without any additive.....	142
5.7	X-ray diffraction scans of $(Sm_{12}Co_{88})_{100-y}C_y$ alloy melt spun at 40 m/s for $y = 0, 1, 2, 3$ and $5$ (from (a) to (e)). Peaks were indexed to the $SmCo_7$ structure.....	144

5.8	Transmission electron micrographs revealing the microstructure of the $(\text{Sm}_{12}\text{Co}_{88})_{100-y}\text{C}_y$ alloy melt-spun at 40m/s (a) for $y=0$ , showing micron scale grains (b) for $y=1$ , showing equiaxed grains (top left inset shows the electron diffraction pattern) and (b) for $y=1$ , showing the smaller grains squeezed by the larger sized grains.....	146
5.9	Transmission electron micrograph revealing the microstructure of the $(\text{Sm}_{12}\text{Co}_{88})_{100-y}\text{C}_y$ alloy melt-spun at 40m/s for $y=3$ showing a mixture of equiaxed grains having a wide range of size distribution.....	147
5.10	Transmission electron micrographs revealing the microstructure of the $(\text{Sm}_{12}\text{Co}_{88})_{100-y}\text{C}_y$ alloy melt-spun at 40m/s for $y=3$ showing (a) leaf-like grains (b) small equiaxed grains and (c) a nice triple point grain boundary.....	148
5.11	Transmission electron micrographs revealing the microstructure of the $(\text{Sm}_{12}\text{Co}_{88})_{100-y}\text{C}_y$ alloy melt-spun at 40m/s for $y=5$ showing (a) very fine strangled dendritic structures, (b) relatively coarser dendritic structures and (c) a mixture of fine and coarse dendrites.....	149
5.12	Hysteresis loops of $(\text{Sm}_{12}\text{Co}_{88})_{100-y}\text{C}_y$ alloy melt spun at 40 m/s for $y = 0, 1, 2, 3$ and 5.....	151
5.13	Relationship between atomic percent carbon added ( $y$ ) and intrinsic coercivity for the $\text{Sm}_{12}\text{Co}_{88}$ alloys - 40m/s modified with C (■).....	152
5.14	The normalised curves showing initial magnetization processes for the $(\text{Sm}_{12}\text{Co}_{88})_{100-y}\text{C}_y$ -40m/s alloys modified with C at different $y$ values $y=1$ (---◇---), $y=2$ (---Δ---), $y=3$ (---□---) and $y=5$ (□) and (+) indicates the sample without any additive.....	153
5.15	X-ray diffraction scans of $(\text{Sm}_{12}\text{Co}_{88})_{100-(x+y)}\text{Nb}_x\text{C}_y$ alloy melt spun at 40m/s for $x=y = 0, 1, 2, 3, 5, 7$ & 10 (from (a) to (g)). Peaks were indexed to the $\text{SmCo}_7$ structure.....	155
5.16	X-ray diffraction scans of $(\text{Sm}_{12}\text{Co}_{88})_{100-(x+y)}\text{Nb}_x\text{C}_y$ alloy melt spun at 40m/s for $x,y=(5,5), (7,7)$ and $(10,10)$ (from (a) to (c)).....	156
5.17	Transmission electron micrographs revealing the microstructures of the $(\text{Sm}_{12}\text{Co}_{88})_{100-(x+y)}\text{Nb}_x\text{C}_y$ alloy melt-spun at 40m/s (a) for $x,y=0,0$ showing large 1:7 grains, (b) for $x,y=0,0$ showing Co precipitates $\sim 80$ nm, (c) for $x,y=3,3$ showing relatively smaller (1:7) grains and (d) for $x,y=3,3$ showing scattered Co precipitates $\sim 10$ nm.....	158
5.18	Transmission electron micrographs revealing the microstructures of the $(\text{Sm}_{12}\text{Co}_{88})_{100-(x+y)}\text{Nb}_x\text{C}_y$ alloy melt-spun at 40m/s (a) for $x,y=7,7$ showing	

	very small sized grains, (b) for x,y=10,10 showing a big oval shaped grain grey in color.....	159
5.19	Demagnetization curves of $(\text{Sm}_{12}\text{Co}_{88})_{100-(x+y)}\text{Nb}_x\text{C}_y$ alloy melt spun at 40m/s.....	161
5.20	Relationship between %additives x and y and intrinsic coercivity for the $(\text{Sm}_{12}\text{Co}_{88})_{100-(x+y)}\text{Nb}_x\text{C}_y$ alloys - 40m/s modified with Nb as well as C.....	162
5.21	The normalised curves showing initial magnetization processes for the $(\text{Sm}_{12}\text{Co}_{88})_{100-(x+y)}\text{Nb}_x\text{C}_y$ - 40m/s alloys modified with Nb as well as C at different (x,y) values (1,1 (♦), 2,2 (■), 3,3 (Δ), 5,5 (×) and 7,7 (▲)) and (+) is indicating the sample without any additive.....	163
5.22	Relationship between lattice parameter and concentration of additives (a) for single additive Nb, (b) for single additive C and (c) for combined additives Nb and C.....	166
5.23	Relationship between grain size and concentration of additives in NbC modified alloys.....	167
5.24	Transmission electron micrograph showing the microstructure of the $(\text{Sm}_{12}\text{Co}_{88})_{100-x}\text{Nb}_x\text{C}_y$ alloy melt-spun at 40m/s for x=3 showing the antiphase boundaries.....	168
5.25	X-ray diffraction scans of the $(\text{Sm}_{11}\text{Co}_{89})_{94}\text{Nb}_3\text{C}_3$ alloys with different wheel speeds (a) 20 m/s, (b) 30 m/s, (c) 40 m/s, (d) 50 m/s and (e) 60 m/s. Peaks were indexed to the $\text{TbCu}_7$ -type $\text{SmCo}_7$ structure.....	171
5.26	Transmission electron micrographs revealing the microstructures of $\text{Sm}_{11}\text{Co}_{89}$ alloy with different wheel speeds (a) 20 m/s, (b) 40 m/s and (c) 50 m/s. The insets are showing the corresponding electron diffraction patterns.....	172
5.27	Relationship between the wheel speeds and intrinsic coercivity for the $\text{Sm}_{11}\text{Co}_{89}$ -NbC alloys.....	174
5.28	The normalised curves showing initial magnetization processes for the $(\text{Sm}_{12}\text{Co}_{88})_{94}\text{Nb}_3\text{C}_3$ alloys melt-spun at different wheel speeds 20m/s (□), 30m/s (♦), 40m/s (■), 50m/s (×) and 60m/s (Δ).....	175
5.29	Relationship between the grain size and the wheel speed of the $\text{Sm}_{11}\text{Co}_{89}$ -NbC Alloys.....	177



5.30	Relationship between the grain size and the coercivity of the $\text{Sm}_{11}\text{Co}_{89}\text{-NbC}$ Alloys.....	177
5.31	X-ray diffraction scans of the $\text{Sm}_{(1/(1+x))}\text{Co}_{(5+x)/(6+x)}\text{Nb}_3\text{C}_3$ with $x=0.67$ to 3 (from (a) to (e)). Peaks were indexed to the $\text{TbCu}_7$ -type structure and $\text{Sm}_2\text{Co}_7$ .....	180
5.32	X-ray diffraction scans of the $\text{Sm}_{(1/(1+x))}\text{Co}_{(5+x)/(6+x)}\text{Nb}_3\text{C}_3$ samples (with $x=0.67$ to 3 from (a) to (e)) in the region where superlattice peaks (notably the (024) of the $\text{Sm}_2\text{Co}_{17}$ structure appear. No (024) peak was observed, indicating the lack of dumbbell ordering.....	181
5.33	Relationship between the lattice parameters, given by $c/a$ , and composition ( $x$ ).....	182
5.34	Transmission electron micrographs revealing the microstructures of alloys with $x=0.67$ , 1.7 and 3 (a, b and c, respectively).....	184
5.35	Demagnetization curves of the sample $\text{Sm}_{(1/(1+x))}\text{Co}_{(5+x)/(6+x)}\text{Nb}_3\text{C}_3$ - 20m/s for (a) $x=0.67$ , (b) $x=1.7$ , and (c) $x=3$ .....	185
5.36	Relationship between composition ( $x$ ) and intrinsic coercivity for the $\text{Sm}_{(1/(1+x))}\text{Co}_{(5+x)/(6+x)}\text{Nb}_3\text{C}_3$ alloys.....	186
5.37	Relationship between composition ( $x$ ) and the magnetocrystalline anisotropy of the $\text{Sm}_{(1/(1+x))}\text{Co}_{(5+x)/(6+x)}\text{Nb}_3\text{C}_3$ alloys. The square end points denote the literature values [5] for the $\text{SmCo}_5$ ( $x=0$ ) and $\text{Sm}_2\text{Co}_{17}$ ( $x=3.5$ ) compounds.....	188
5.38	The maximum energy product $(BH)_{\text{max}}$ and the remanence ( $M_r$ ) for the $\text{Sm}_{(1/(1+x))}\text{Co}_{(5+x)/(6+x)}\text{Nb}_3\text{C}_3$ alloys.....	189
5.39	X-ray diffraction scans of (a) the as-solidified $\text{Sm-Co-Nb-C}$ alloy ( $\text{Sm}_{12}\text{Co}_{88}$ ), and after heat treatment at (b) $700^\circ\text{C}$ , (c) $800^\circ\text{C}$ , and (d) $900^\circ\text{C}$ . (e) Calculated diffraction pattern for $\text{Sm}_2\text{Co}_{17}$ . The figure at right top corner shows the electron diffraction pattern.....	193
5.40	X-ray diffraction scans of the $\text{Sm-Co-Nb-C}$ alloy ( $\text{Sm/Co}=9/91$ , i.e. $x=5.1$ ), after heat treatment at $900^\circ\text{C}$ for (a) 15 minutes, (b) 30 minutes and (c) 45 minutes.....	194
5.41	X-ray diffraction scans of the $(\text{Sm}_{(1/(6+x))}\text{Co}_{(5+x)/(6+x)})_9\text{Nb}_3\text{C}_3$ alloys annealed at $900^\circ\text{C}$ and for 15 minutes, for different compositions (a) $x=2.3$ , (b) $x=3$ , (c) $x=4$ , (d) $x=5.1$ and (e) $x=5.7$ . (f) Calculated diffraction pattern for $\text{Sm}_2\text{Co}_{17}$ .....	195

5.42	Transmission electron micrographs revealing the microstructures of $\text{Sm}_{12}\text{Co}_{88}$ alloy melt spun at 40m/s and annealed at (a) 800°C (b) 900°C.....	197
5.43	Relationship between annealing temperature and intrinsic coercivity for the ribbons having different compositions $x=2.3$ (■), $x=3$ (▲), $x=4$ (◆), $x=5.1$ (▲) and $x=5.7$ (◆).....	198
5.44	Relationship between composition and intrinsic coercivity for as-solidified ribbons (◆) as well as annealed ribbons (-■-) achieving maximum coercivity.....	200
5.45	The normalized curves showing initial magnetization behavior at different annealing temperatures (▲ as-solidified, ■ 900°C and ◆ 800°C).....	201
5.46	The normalized curves showing initial magnetization behavior at different Sm/Co ratio $x=2.3$ (◆), $x=3$ (×), $x=5.1$ (■) and $x=5.7$ (▲), annealed at 800°C.....	203
5.47	The curves showing normalized remanent susceptibility of $\text{Sm}_{12}\text{Co}_{88}$ sample melt-spun at 40m/s and annealed at three different temperatures (a) 700°C, (b) 800°C and (c) 900°C. The inset is showing an expanded view of the region from 0kOe to -5kOe.....	204
5.48	Three reversible magnetization curves showing different nucleation and pinning density for sintered Nd-Fe-B magnets [10].....	205
5.49	The $M_{\text{rev}}$ Vs. $M_{\text{irr}}$ curves showing reversibility-irreversibility of the sample $\text{Sm}_{12}\text{Co}_{88}$ melt-spun at 40m/s at different annealing temperatures (a) 700°C, (b) 800°C and (c) 900°C at a field of 2000 Oe.....	207
5.50	The $M_{\text{rev}}$ Vs. $M_{\text{irr}}$ curves showing reversibility-irreversibility at different fields of the two sets of the samples (a) $\text{Sm}_{12}\text{Co}_{88}$ and (b) $\text{Sm}_9\text{Co}_{91}$ melt-spun at 40m/s annealed at 800°C.....	208
5.51	Transmission electron micrographs revealing the microstructures of $\text{Sm}_{12}\text{Co}_{88}$ alloy melt spun at 40m/s and annealed at 800°C (a) bright field image and (b) dark field image.....	210
5.52	The selected area diffraction pattern for the $\text{Sm}_{12}\text{Co}_{88}(\text{NbC})$ -40 m/s sample annealed at 800°C.....	211

## LIST OF TABLES

1.1	The crystal structures and magnetic properties of various permanent magnets .....	4
2.1	Magnetocrystalline Anisotropy constants for some important magnetic materials at room temperature [22] .....	26
3.1	Magnetic Properties and Chemical Compositions of Rare-earth-Transition Metal Systems [9] .....	69
3.2	The Magnetic Properties of Some $RCO_5$ Phases [15] .....	72
3.3	Important Magnetic Properties of Several $R_2A_{17}$ Compounds, $A=Fe$ and $Co$ [28] .....	76
3.4	Magnetic Properties of $SmCo_5$ and $Sm_2Co_{17}$ families.....	82
4.1	Raw Materials Procured For The Experiments.....	100
5.1	Magnetic Properties of the $Sm_{12}Co_{88}$ Alloys Modified With $Nb$ and/or $C$ .....	164
5.2	The Structures and The Magnetic Properties of The $Sm_{11}Co_{89}$ Alloys at Different Wheel Speeds.....	176

## ACKNOWLEDGEMENTS

I would like to express my heartiest appreciation to my thesis advisor Professor Jeffrey E. Shield for his constant guidance and support in carrying out this research work. I also wish to thank to Professor Brian W. Robertson, Professor Diandra L. Pelecky and Professor Jennifer I. Brand for their assistance as my supervisory committee.

I would like to extend my special thanks to Dr. Jian Jhou and Dr. Korey Dean Sorge for their help in carrying out a part of my experimental work. I owe thanks to all my colleagues in my research group for being a source of encouragement and support through out this research work.

Last but not least, I want to express my immense appreciation to my father Mr. Paritosh Kumar Aich and my friend Ms. Banasri Roy who have been my biggest supporters throughout my Ph.D career.

This work was supported by the National Science Foundation under Grant No. DMR0305354. The author is grateful to the Center for Materials Research and Analysis and MRSEC: QSPINS (NSF grant no. 0213808) for facility support. Many useful discussions with Dr. L.H. Lewis, Dr. R. Skomski and Dr. R.W. McCallum are gratefully acknowledged.

## **CHAPTER I :: INTRODUCTION**

### **1.1 Significance of The Study**

Since the discovery of the naturally occurring mineral, magnetite ( $\text{Fe}_3\text{O}_4$ ), magnetism and magnetic materials have been playing an important role in modern science and technology. In ancient times, the Chinese and the Greeks were using lodestones or “waystones” in guiding mariners. In 1600, physicist, William Gilbert, experimented with lodestone, iron magnets and the magnetic field of the earth. His experiments laid the foundation for current scientific applications, and dispelled the folklore surrounding magnetism and magnetic material [1]. Research about magnetic materials expanded after the invention of electromagnets by physicist Hans Christian Oersted in 1820 [1]. Permanent magnets have brought much more attention to the field, because unlike powerful electromagnets, they can be used without any consumption of electricity or generation of heat.

Permanent magnets are used and extensively studied in academic and military research and energy laboratories. Another important area of application is in medical industries (MRI, hematology laboratories and magnetic hyperthermia technique). About 160 magnets are used for different purposes in our daily lives. The applications range from refrigerator magnets, kitchen appliances, television, telephone, watches, computer, audio systems, to microelectronics. Another 100 magnets are used in the automobile industry. Permanent magnets are behind some of the most important inventions of our modern lives. They make our lives pleasant, comfortable and easier. They have a promising future, because a number of new devices are waiting for them. Ultimately,

there is a basic necessity to understand and improve their properties, as well as to look for new applications for them.

The first commonly used permanent magnets were made of carbon steel and were shaped like a horseshoe. Although this type of magnet is now obsolete, the horseshoe represents the symbol for magnetism [2]. In the past sixty years the applications of permanent magnets have been diversified due to discoveries of new materials like Alnicos (alloys of Al, Ni, Co and Fe), ferrites (combination of iron oxide with another metal), Nd-Fe-B and Sm-Co magnets. Although the Alnicos were extensively used in the mid-twentieth century as general-purpose permanent magnets, for their moderate magnetic properties achieved by relatively easy processing, they were replaced by much cheaper ferrites which now occupy 55% of the permanent magnet world market.

The field of rare-earth permanent magnets was initiated by the discovery of  $\text{SmCo}_5$  in the late 1960s. People were much more attentive to these Sm-Co magnets due to their high anisotropy field  $H_A$ . The anisotropy field was twice that of the contemporary ferromagnetic Alnico alloys. A higher anisotropy field increases the coercivity  $H_{ci}$ , which helps to increase the maximum energy product  $(BH)_{\max}$ , the amount of energy stored inside the material, which is the maximum value of the product of the magnetic induction (B) and the applied field (H) in the second quadrant of the B versus H hysteresis curve (will be discussed in detail in the next chapter – Chapter II). However, to avoid using relatively expensive and vulnerable sources of Co, the search for the Fe-based permanent magnets continued. This led to the discovery of  $\text{Nd}_2\text{Fe}_{14}\text{B}$ -based materials in 1983, followed by interstitially modified Sm-Fe-N in 1992. But, both of these have some drawbacks compared to Sm-Co magnets. The Sm-Fe compounds are not useful as

permanent magnet materials (for their basal plane easy magnetization direction) unless nitrogen diffusion expands the crystal structure and produces  $\text{Sm}_2\text{Fe}_{17}\text{N}_x$ . The Nd-Fe-B magnets are not applicable at higher temperatures. Table 1.1 displays representative properties of various permanent magnet materials.

As the second generation of rare-earth permanent magnets, Sm-Co-based magnets have been available since the early 1970's. The most interesting features of these magnets are high energy products (14 MGOe – 30 MGOe), reliable coercive force and the best temperature characteristics in the rare-earth materials family. Sm-Co-based magnets not only have better corrosion and oxidation resistance, but also exhibit better temperature stability. This is the ideal material in applications such as pump couplings, sensors and servo-motors. The Sm-Co system forms two related equilibrium phases in Co-rich compositions: the  $\text{CaCu}_5$ -type  $\text{SmCo}_5$  structure and the  $\text{Th}_2\text{Zn}_{17}$ - or  $\text{Th}_2\text{Ni}_{17}$ -type  $\text{Sm}_2\text{Co}_{17}$  structure. The  $\text{CaCu}_5$  structure itself is rather simple, with one Ca (R) site and two distinct Cu (Co) sites. The  $\text{Sm}_2\text{Co}_{17}$  structure is related to the  $\text{SmCo}_5$  structure through the ordered substitution of one Sm by a pair of Co atoms (commonly referred to as Co dumbbells) [3]. In addition to the ordered  $\text{Sm}_2\text{Co}_{17}$  dumbbell structures, the dumbbell arrangement can be randomized on the rare earth sites as the disordered  $\text{TbCu}_7$ -type structure [4]. This metastable structure has the same unit cell as the  $\text{CaCu}_5$  structure. The suppression of the long-range order, leading to the formation of the  $\text{TbCu}_7$ -type  $\text{SmCo}_7$  structure, has been accomplished by melt spinning [5], splat cooling [6], mechanical alloying [7], and dilute additions of Zr and Ti [8,9,10]. The formation of

Table 1.1 The crystal structures and magnetic properties of various permanent magnets.

Property	Alnico	BaFe <sub>12</sub> O <sub>19</sub>	SmCo <sub>5</sub>	Nd <sub>2</sub> Fe <sub>14</sub> B	Sm <sub>2</sub> Fe <sub>17</sub> N <sub>x</sub>
Structure	cubic	hexagonal	hexagonal	tetragonal	Rhombohedral
Anisotropy field H <sub>A</sub> (kOe)	5		350	80	140
Saturation magnetization 4πM <sub>S</sub> (kG)	19	6.3	11	16	15.4
Curie temperature T <sub>C</sub> (K)	1120	745	1000	580	770
Maximum energy product (BH) <sub>max</sub> (MGOe)	5.5	4.3	18.1	36.4	10.936

the disordered SmCo<sub>7</sub> structure has provided pathways to the development of materials with novel structures, as exemplified by recent advancements in the elevated-temperature performance of Sm-Co-based materials.